Applied Catalysis B: Environmental 129 (2013) 528–538

Contents lists available at SciVerse ScienceDirect

Applied Catalysis B: Environmental

journal homepage: www.elsevier.com/locate/apcatb

Gas-phase hydrodeoxygenation of guaiacol over iron-based catalysts. Effect of gases composition, iron load and supports (silica and activated carbon)

R. Olcese[a], M.M. Bettahar[b,*], B. Malaman[c], J. Ghanbaja[c], L. Tibavizco[a], D. Petitjean[a], A. Dufour[a,*]

[a] LRGP, CNRS, Université de Lorraine, ENSIC, 1, Rue Grandville, Nancy, France
[b] SRSMC, CNRS, Université de Lorraine, Faculté des Sciences, Bvd. des Aiguillettes, 54506 Vandoeuvre-les-Nancy, France
[c] IJL, CNRS, Université de Lorraine, Faculté des Sciences, Bv. Des Aiguillettes, Vandoeuvre-les-Nancy, France

ARTICLE INFO

Article history:
Received 27 June 2012
Received in revised form 31 August 2012
Accepted 26 September 2012
Available online 5 October 2012

Keywords:
Biorefinery
Lignin
Hydrotreatment
Chemicals
Aromatic

ABSTRACT

Fe/SiO_2 is shown to be a selective catalyst for guaiacol hydrodeoxygenation (HDO). Guaiacol is used as a model compound to study the conversion of lignin pyrolysis vapours into aromatics (benzene, phenols). The effect of each individual gas present in a pyrolysis gas (H_2, CO, CO_2, H_2O, CH_4) on the selectivity of a 10 wt% Fe/SiO_2 catalyst is studied (673 K, atmospheric pressure, 50 mol% H_2, 1/WHSV = 0.6 g_{cat} h/g_{gua}). The speciation of the iron phase (metallic (α-Fe), carbide (Fe_5C_2), oxide (Fe_3O_4), and super-paramagnetic) in spent catalysts is revealed by XRD and Mössbauer spectroscopy as a function of gases composition. At least 3 types of carbonaceous deposit were evidenced by TPO analysis. TEM observations showed that iron particles size is not markedly affected by the reaction and that carbon deposit mainly occurs in the vicinity of iron particles. When all the gases except methane (Guaiacol + H_2 + CO + CO_2 + H_2O) are simultaneously in the feed stream, the conditions are still sufficiently reducing to maintain the activity of the catalyst (66% of benzene and toluene carbon yield, 7.5 g_{cat} h/g_{gua}). The effects of support (silica or activated carbon-AC) and iron loading (5, 10, 15 wt% Fe/SiO_2) were also studied. 10 wt% Fe/AC has a higher selectivity in phenol and cresols production than Fe/SiO_2. Active sites and reaction mechanisms are discussed.

1. Introduction

Lignin output would be very abundant in future biorefinery [1]. Lignin is currently valorised by combustion in the pulp industry. However, lignin could be transformed to value added chemicals, due to its aromatic structure. Aromatic compounds, oxygenated (phenols) or not (BTX: benzene, toluene and xylenes), are valuable chemicals and building blocks with very developed markets [1]. Fast pyrolysis of lignin appears as an interesting first step in the conversion of lignin to aromatic chemicals. Lignin pyrolysis vapours are composed of a huge variety of aromatic compounds with a high amount of oxygenated groups (mainly hydroxyls and methoxyls) [2]. This complex mixture of oxygenated aromatics is unstable because of repolymerisation reactions that form useless solid lignin oligomers [3,4]. To our point of view, the gas-phase conversion downstream the pyrolysis reactor of oxygen-rich aromatic compounds into a less complex mixture of more stable aromatic chemicals could be a preferred route (Fig. 1) compared with a liquid-phase conversion of reactive liquids after a condensation of pyrolysis vapours.

Hydrodeoxygenation (HDO, hydrogenolysis of C—O linkage) appears as a potential route for reducing the oxygen content of bio-oils. Most HDO catalyst and processes were developed for high pressures (50 bar) of pure H_2 and temperatures about 473–573 K [5,6], typical of crude oil hydrotreatment. The case of lignin pyrolysis vapours (typically from a fluidized bed) is very different: pressure is close to 1 bar, temperatures are about 573–773 K and the gas stream is diluted in fluidization gas and other gases produced from lignin pyrolysis (CO_2, H_2, CO, CH_4) [2]. An important issue is that the catalytic reactor coupled to the pyrolysis reactor should be at around 673 K if a minimum condensation of vapours before the catalytic reactor is looked for. The selectivity of the catalyst should be set for these conditions. Some precious very active catalysts could lead to a bad selectivity (such as methane production with high consumption of H_2) if used at 673 K [7].

In a lignocellulosic biorefinery, it is expected to have a reduction gas with a certain percentage of H_2 (diluted in CO_2, CO, N_2 and CH_4) from biomass gasification [8] or reforming of biobased compounds [9,10], rather than technically pure H_2, typical of crude oil hydrotreatment. An extra issue is that pyrolysis of lignin could produce heavy lignin oligomers that will plug a catalyst fixed-bed.

* Corresponding authors. Tel.: +33 383175078.
E-mail addresses: mohammed.bettahar@lcah.uhp-nancy.fr (M.M. Bettahar), anthony.dufour@univ-lorraine.fr (A. Dufour).

0926-3373/$ – see front matter © 2012 Elsevier B.V. All rights reserved.
http://dx.doi.org/10.1016/j.apcatb.2012.09.043

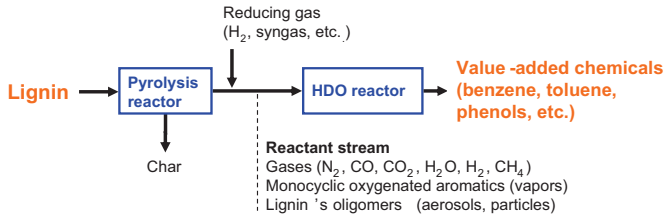

Fig. 1. Lignin conversion to aromatics compounds via catalytic treatment of pyrolysis vapours.

Innovative catalytic process must be developed in order to overcome these problems.

Literature about HDO on the liquid phase is very abundant, see [5,6] for review. However, at gas-phase, low pressure and temperatures close to 673 K (i.e. lignin pyrolysis conditions), there are fewer works than for high-pressure HDO. Table 1 is a selection of some literature data concerning this subject for phenolic compounds (considering BTX and phenol as the goal).

Lignin pyrolysis vapours will form carbon deposits on all kind of solids due to aerosols, coke formation (etc.). Consequently, the desired characteristics of a lignin pyrolysis HDO catalyst are: low price, easy regeneration and selectivity to stable aromatics even in presence of other pyrolysis gases. Shin and Keane [11] compared the conversion of phenol over Ni/SiO_2 using methanol-water mixtures as solvent. It was shown that water shifted selectivity from hydrogenolysis products (benzene) to ring hydrogenation products (cyclohexanol). Zhu et al. [15] injected water during an experiment of anisole HDO on Pt/HBeta zeolite. They found that anisole conversion is accelerated, but that hydrolysis products are formed. Besides these works and to the best of our knowledge, there is not yet works about the effect of other pyrolysis gases (CO, CO_2, etc.) on the gas phase catalytic HDO of lignin pyrolysis model compounds.

In previous works [7,19], we showed that a catalyst as simple as iron supported on silica was active and selective for guaiacol conversion to benzene and toluene, but a commercial cobalt catalyst was not, because C—C linkages of guaiacol were hydrogenated and methane was produced. Fe/SiO_2 catalyst is selective because it does not catalyze the hydrogenation of the aromatic ring.

In the present paper, we focus on the effect of CO, CO_2, CH_4 and H_2O, gases present in the lignin pyrolysis vapours, on the HDO of guaiacol over Fe/SiO_2. The concentrations of the gases were chosen in order to mimic the real process conditions. It is a first step towards the development of a catalytic reactor coupled to real pyrolysis gases. We are aware that in a real pyrolysis gas other species such as heavy lignin oligomers should also impact catalyst activity [2,20]. For a better understanding of the catalytic mechanisms, the individual behaviour of the gases was studied in the presence of guaiacol and the hydrogenation of CO and CO_2 were performed in the absence of guaiacol. We also performed experiments with different loads of iron on silica, and also using activated carbon as support (instead of silica). The influence of the mass of catalyst was specifically studied at high HDO conversions in order to ensure that aromatic hydrocarbons are not further converted.

Catalyst deactivation is an important point for this reaction [15,20]. Consequently, characterizations were made on used catalysts (XRD, Mössbauer, TEM, and Temperature Programmed Oxidation-TPO).

2. Experimental

2.1. Catalyst preparation

Iron over silica (Fe/SiO_2) catalyst was prepared by simple impregnation [19]. 7 g of silica (Aerolyst 3039, Degussa; grounded and sieved 63–250 μm) were contacted with 21 ml of an iron nitrate nonahydrate (Sigma) solution in deionised water. The mixture was exposed to vacuum at room temperature for 3 h, and then dried 24 h at 373 K. The resulting impregnated solid was regrounded and sieved (63–250 μm), and then treated under Argon flow (50 Nml/min) with temperature increasing from 298 K to 773 K at 5 K/min and hold at 773 K for 1 h. The amount of iron nitrate nonahydrate diluted on water was tailored to reach 5, 10 and 15 wt% Fe on the reduced catalyst. Iron loadings were checked by elemental analysis and calculated assuming that Fe_2O_3 (given by the elemental analysis) is completely reduced. 4.9, 9.5 and 14.7 wt% of iron loads (if assumed reduced) have been quantified. Iron over carbon catalyst was prepared by the same method, but using activated carbon NORIT RX-3 "Extra" as support.

The argon-treated catalyst was reduced in situ by pure H_2 (50 ml/min) before guaiacol HDO. Temperature was increased from 298 K to 773 K at a rate of 5 K/min, then hold 773 K during 1 h. The reactor feed was then changed to hydrogen-argon mix at desired flows and H_2 molar fraction. The temperature was set to 673 K (reaction temperature). After a stabilisation time (50 min), guaiacol syringe pump, water syringe pump and/or other gases (CO, CO_2, CH_4) mass flow controllers were turn on. The start of the catalytic run was considered from guaiacol injection.

Fresh passivated catalysts were also prepared for further analysis. 200 mg of argon-treated catalyst were placed in a fixed bed reactor and flowed with 50 Nml/min of H_2. Temperature was raised from 298 K to 773 K at a rate of 5 K/min, then hold at 773 K for 1 h. Sample was then left to cool to room temperature (293 K) under 50 Nml/min of Argon. Gas inlet was switched to 50 Nml/min of a mixture of 100 ppm of O_2 in Argon and this condition was maintained for 1 h before exposing the catalyst to air. Otherwise, the reduced non passivated material was highly pyrophoric. However, used catalysts for HDO reaction did not show pyrophoric character, and they were analysed without passivation.

2.2. Catalytic runs

The experimental set-up has been previously presented [19]. Guaiacol was purchased from Sigma Aldrich. Ar and H_2 were purchased from Messer, CO, CO_2 and CH_4 from Air Liquide. Ar, H_2, CH_4, CO and CO_2 were introduced by five Mass Flow Controllers (Bronkhorst). Guaiacol and water were injected by means of two syringe pumps. All runs were made on a fixed-bed catalytic reactor. The conditions for all runs were $P = 1–1.1$ bar, $T = 673$ K, $F_v = 40$ Nml/min (total volume flow rate), particle size 63–250 μm. All runs lasted 187 min, and the concentration of aromatics reactants and products were analyzed 5 times along time on stream (each 42 min). Low conversion experiments were conducted in a 4 mm i.d. quartz tube where 48–154 mg of catalyst were handled between two plugs of quartz wool. High HDO conversion experiments were made in 8 mm i.d. pyrex tube where 1000–1200 mg of catalyst were fixed between wool plugs. Products were piped (at 483 K to avoid condensation) to a 6 ways sampling valve (at 508 K) connected to a Gas Chromatograph (Varian 3800) equipped with a DB-1701 column (60 m, ID 0.25 mm, 0.25 μm, cyanopropylphenyl–14%/dimethylsiloxane–86%) and a FID detector. The sample in the heated loop was injected with a split ratio of 20. Injection temperature was 250 °C and GC furnace temperature program: heating from 60 °C to 155 °C at 6 °C/min; then from 155 °C to 175 °C at 2 °C/min; then from 175 °C to 270 °C at 10 °C/min and hold 1 min at 270 °C. This chromatographic method allows a good separation of products and a relative fast elution (42 min between each analysis including cooling) for on-line analysis. Relative response factors were calculated from standard mixtures by means of liquid injection, with very good reproducibility (relative standard deviation of 3 injections lower than 5% for each product).

Table 1
Selected results from literature on phenolic compounds gas-phase HDO.

References	Catalyst	Phenolic molecule	Conditions	Results
[11,12]	Ni/SiO_2 (loads from 1.5 to 20 w%), Ni/Na-Y zeolite. Ni/SiO_2 and Pd/Al_2O_3 doped with Na, K, Cs, Mg, Ca, Sr, and Ba	Phenol	573 K, C_{PhOH} = 9%; C_{MeOH} = 36%	Yield $_{Benz}$ = 99%; on 20 w% Ni loads. Group I and II metal addition promotes ring hydrogenation.
[13–15]	Pt-Sn/CNF; Pt, Sn, Pt-Sn (monolith-supported); Pt/(Hbeta, SiO_2)	Guaiacol; anisole	673 K, $C_{Gua\ or\ Anisole}$ = 0.6–2%	$Yield_{BTX}$ = 85% (anisole on Pt/HBeta). $Yield_{BTX}$=60% (guaiacol on Pt-Sn/CNF)
[16]	M-P/SiO_2 (M: Ni, Fe, Co, Mo, W); Pd/Al_2O_3	Guaiacol	573 K, C_{Gua} = 0.024%	$Yield_{BTX}$ = 60% on Ni_2P catalyst
[17,18]	MoS_2, CoMo-CoMoS supported on Al_2O_3, TiO_2 or ZrO_2)	Guaiacol	573 K, 40 bar, C_{Gua} = 0.07%; C_{H2S} = 0.01%	ZrO_2 was the best support for production of BTX.

The absolute response of the on-line sampling system was measured by injecting guaiacol and methanol into the reactor without catalyst at 623 K and under argon flow (blank test). The areas of guaiacol (for blank test) showed a standard deviation of 8% for ten GC-FID analysis with the sampling loop.

The exit gases from the sampling valve was connected to a first glass bubbler filled by 2-Propanol at 273 K and then to a second bubbler at 213 K to protect the μGC from condensable heavy products. Incondensable products (methane, ethane, CO, CO_2, etc.) were analyzed on-line with a μGC-Varian 490 equipped with four modules (four columns with four thermal conductivity detectors) connected to the exit of the bubblers. The four modules were composed of two molecular sieves 5A, a PoraPlot U and a CP–Wax 52CB columns. μGC-490 signal was calibrated using four standard bottles (Air Liquide, France).

2.3. Characterization of the fresh passivated and spent catalysts

The load in iron of catalysts was checked by ICP-MS analysis (CNRS-SARM procedure [21]). The samples have been analysed by conventional X-ray powder analysis (XPERT Pro Cu Kα) and the crystal structures have been refined using the Fullprof software [22]. The ^{57}Fe Mössbauer measurements were carried out using a constant-acceleration spectrometer in standard transmission geometry with a ^{57}CoRh source (25 mCi). Spectra were recorded at 300 K. A polycrystalline absorber with natural abundance of ^{57}Fe isotope and thickness of ~15 mg cm^{-2} was used. The Mössbauer spectra were fitted with a least-squares method program assuming Lorentzian peaks.

Temperature programmed oxidation (TPO) was performed on a 4 mm i.d. quartz tube. Between 30 and 40 mg of sample were placed between two quartz wool plugs and flowed by air (50 Nml/min). Temperature was increased from 293 to 1023 K at 5 K/min. Produced carbon dioxide was measured on-line by the μGC. Carbon monoxide was not detected.

Transmission electron microscopy (TEM) imaging was performed with a Philips CM20 (200 kV) microscope, equipped with an EDXS spectrometer.

2.4. Evaluation of catalytic runs

For all runs, the aromatic ring balance (aromatic ring in analysed product/aromatic ring injected from guaiacol) was between 75 and 95% (mol based), depending on coke deposition conditions. For blank test, guaiacol molar balance was between 95 and 104%.

Yield of products (Y_i) was calculated using Eq. (1), where C_i is the molar percentage of the product i and X is the conversion of guaiacol. C^0_{gua} is the initial molar percentage of guaiacol, and was equal to 1 mol% for all runs.

$$Y_i(\%) = \frac{C_i(\text{mol}\%)}{C^0_{gua} \cdot X_{gua}} \quad (1)$$

The total amount of guaiacol converted on a 187 min experiment was calculated by integration of the five (along time on stream) GC-FID on-line analysis. Weighted mass of oxidised catalyst is used to calculate 1/WHSV. However, the weighted catalyst is Fe_2O_3/SiO_2. Considering the loss of oxygen atoms due to reduction, a correction factor must be added to calculate the exact mass of catalyst in the reactor (in the worst case 15 wt% Fe/SiO_2 the correction factor is 0.96).

The size of iron particles supported on silica and activated carbon was measured by TEM images. For passivated and used catalyst, 3 images were selected and 10–15 particles were measured manually for each image and all results were averaged. The iron available surface was calculated considering full exposed perfect spheres of regular diameter. We are aware that it is needed to count more particles to get a precise size distribution of particle diameter, but the agreement between TEM and XRD is reasonable.

For the TPO experiment, the raw CO_2 molar fraction was treated as follows. Initial CO_2 molar fraction in air (0.038%) and baseline were subtracted. The resulting data contained negative points that were replaced by zero. Finally, the CO_2 flow data was integrated numerically (Eq. (2)) to calculate coke mass fraction (w%) on spent catalyst. Then it was referred to initial mass of catalyst of the catalytic run to calculate coke yield. A numeric example is presented in supplementary material.

$$n^{\text{Cat run}}_{\text{Carbon deposit}}(\mu\text{mol}) = \int (F_v.C_{CO_2})_{TPO} \cdot \frac{W^{\text{Cat run}}_{Fe/SiO_2 fresh}}{W^{TPO}_{Fe/SiO_2 spent} \cdot \left(1 - \frac{w\%_{Coke}}{100}\right)} \quad (2)$$

3. Results

3.1. Characterization of fresh passivated catalysts

Initial BET specific surface area of silica was 250 m^2/g. However, measured specific surface area of the impregnated catalyst (without reduction) was about 144 m^2/g. Textural structure of silica is clearly modified by the method of catalyst preparation.

Table 2 and Fig. 2 display the Mössbauer and XRD characterizations of fresh–passivated and used catalysts. Only the composition of the fresh catalysts is discussed in this section.

The XRD pattern of the fresh passivated 10% Fe/AC catalyst essentially shows the diffraction peaks corresponding to α-Fe (Fig. 2a) and some very large diffusion peaks. The corresponding Mössbauer spectrum exhibits the characteristic sextuplet of α-Fe (with line widths of 0.4–0.6 mm/s corresponding to small particles ~15 nm and a proportion area of 35%, Table 2) and a central doublet with hyperfine parameters of about IS = 0.3 mm/s, QS = 0.9 mm/s assigned as Fe^{3+} species (Table 2). Mössbauer spectra and fits are discussed in supplementary material. Galuszka et al. [23] found also this signal in Fe/SiO_2 catalyst and proposed that this may be caused by very little particles of hematite (α-Fe_2O_3; <13 nm) and/or lepidocrocite γ-FeOOH. They explain the presence of this oxidized iron forms as a consequence of the passivation process and exposure to

Table 2
Mössbauer hyperfine parameters of different catalysts.

Catalyst	Species	IS (mm/s)	QS (mm/s)	H (kG)	Area (%)	Molar percentage of species (mol%)
10% Fe/AC fresh and passivated.	α-Fe	0	0	330	35	60.6
	Fe^{3+}	0.34	0.92	0	65	39.4
15% Fe/SiO_2 fresh and passivated.	α-Fe	0	0	331	42	71.0
	Fe^{3+}	0.35	0.9	–	29	17.1
	Fe_3O_4	~0.3	~0	465	20	8.2
	Superpara	–	–	–	9[a]	3.7
10% Fe/SiO_2	α-Fe	0	0	329	18	48.2
Gua + H_2 + CO + CO_2 + H_2O high	Fe^{3+}	0.37	0.95	–	12	11.2
benzene yield	χ-Fe_5C_2	0.25	0.09	210		
	χ-Fe_5C_2	0.2	0.06	190	30	14.8
	χ-Fe_5C_2	0.22	0.08	116		
	Superpara				40[a]	25.8
10% Fe/SiO_2 Gua + H_2 + CO	Fe^{3+}	0.3	0.9	–	28	42.5
	χ-Fe_5C_2	0.25	0.09	209		
	χ-Fe_5C_2	0.2	0.06	183	72	57.5
	χ-Fe_5C_2	0.22	0.08	109		
10% Fe/SiO_2 Gua + H_2 + CO_2	α-Fe	0	0	329	26	59.6
	Fe^{3+}	0.37	0.95	0	24	19.2
	χ-Fe_5C_2	0.25	0.09	210		
	χ-Fe_5C_2	0.2	0.06	183	50	21.1
	χ-Fe_5C_2	0.22	0.08	110		

[a] Calculated by difference. Mössbauer spectra and fits are discussed in supplementary material. Assuming the Lamb Mössbauer factor effect similar for all species. Mole fractions of species were calculated assuming Fe^{3+} as Fe_2O_3 and Superpara as Fe_3O_4.

humid air. It is worth noting that we observe the presence of this doublet (with various intensities) in all the five studied samples, the linewidth of this Fe^{3+} doublet going from 0.5 to 0.85 mm/s.

The XRD pattern of the fresh passivated 15% Fe/SiO_2 is totally indexed as α-Fe and magnetite Fe_3O_4 (Fig. 2b). The corresponding Mössbauer spectrum is in fair agreement with these conclusions. Nevertheless, very broad peaks, at the highest velocities, and a large doublet, in the central part, complete the spectrum. The external peaks correspond to ordered magnetites with various grain sizes [24] and the central doublet to Fe^{3+} species as previously observed in the 10% Fe/AC catalyst sample (Table 2). However, this fit could not explain the whole observed absorption area, and the difference was ascribed as superparamagnetic particles of magnetite [25]. Details of fitting and discussion are presented in supplementary material. Our analysis shows that α-Fe remains the major iron species (on a molar basis, Table 2) in both fresh passivated catalysts.

Passivated fresh catalysts were characterized by TEM (Fig. 3a–d). Table 3 summarizes the result of particle size analysis. It is observed that iron particles are mainly spherical, and that silica has a colloidal structure. The average iron particle size on silica shows little deviations for the three silica loads. On the other hand, TEM micrographs showed clearly that activated carbon-supported iron particles are bigger than silica-supported ones, probably due to different surface oxygen functionalities on activated carbon that leads to a more hydrophobic support than silica and reduces catalyst dispersion [26].

Crystallite average size was calculated using Scherrer's equation at $2\theta = 44.7^\circ$ peak. It yielded 17 nm for 15% Fe/SiO_2 catalyst and 20 nm for 10% Fe/AC. For 15% Fe/SiO_2, the agreement between TEM and XRD particle size analysis is reasonable. However, the 10% Fe/AC crystallite size deduced from XRD was lower than that observed by TEM. It is possible that iron is supported on carbon as agglomerates.

Table 3
Characterization of fresh passivated catalysts from TEM and XRD analyses.

Catalyst	Iron particle size from TEM (nm)	Iron crystallite size from XRD[a] (nm)
5% Fe/Silica	13	Not analyzed
10% Fe/Silica	18	Not analyzed
15% Fe/Silica	14	17
10% Fe/AC	29	20

[a] Based on Scherrer's equation at $2\theta = 44.6^\circ$ ($K = 0.9$).

3.2. Hydrogenation of CO and CO_2 without guaiacol

Before performing guaiacol hydrotreating tests in the presence of different gases, the activity of 10% Fe/silica catalyst on CO_2 and CO hydrotreatment was evaluated. Figs. 4 and 5 show experimental data for these reactions. Results are in agreement with literature for CO [27] and CO_2 hydrogenations [28].

When CO_2 was the reactant, CO was the major product from CO_2 hydrogenation (reverse water–gas shift: $CO_2 + H_2 = CO + H_2O$). For both CO and CO_2 (in H_2), methane was the most important hydrocarbon product. Ethane and ethylene were also detected (from the methanation reactions). These reactions are not desirable, since they consume hydrogen uselessly and they produce carbon deposits on the catalyst.

Since CO_2 hydrogenation produced mainly CO, the reactivity of CO + H_2 on 10% Fe/SiO_2 was studied under the same conditions. When CO is the reactant, the CO conversion decreases drastically in the first minutes of reaction, and considerable amounts of carbon deposit were analyzed by TPO (see Section 3.3). CO_2 is produced probably from CO dismutation [27]. CO conversion (in H_2) decreases drastically whereas CO_2 conversion (in H_2) is more stable. CO conversion could lead to a faster deactivation of the catalyst than CO_2. The effect of CO and CO_2 on the composition of the catalyst and its deactivation is discussed in the following section.

3.3. Individual effect of CH_4, H_2O, CO_2 and CO on guaiacol HDO and used catalysts composition

SiO_2 without iron was inactive for guaiacol conversion (100 mg, 1% Gua, 50% H_2 rest Ar). Activated carbon (without iron) showed a very low activity ($X_{gua} < 5\%$; 100 mg, 1% Gua, 50% H_2 rest Ar). Fe_3O_4/SiO_2 showed very low activity ($X_{gua} < 5\%$; 100 mg, 1% Gua, 50% H_2, 5% CO_2, 2% CO, 2% H_2O, rest Ar, 673 K). Guaiacol conversion was conducted with a higher H_2O/H_2 ratio of 10/50 mol%. (rather

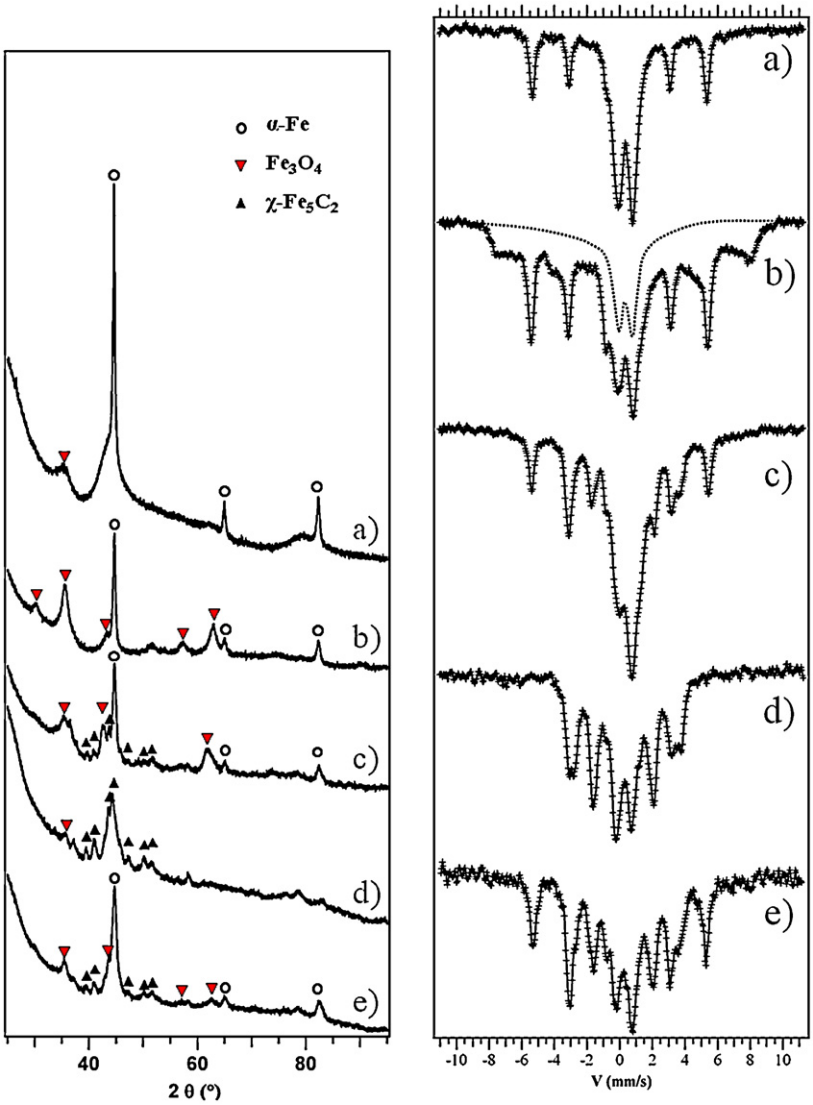

Fig. 2. XRD patterns and ^{57}Fe Mössbauer spectra (recorded at 300 K): (a) Fresh and passivated 10% Fe/AC; (b) fresh and passivated 15% Fe/SiO_2; (c) 15% Fe/SiO_2 from high conversion experiment (Gua + H_2 + CO_2 + CO + H_2O, see text for conditions); (d) 10% Fe/SiO_2 from Gua + H_2 + CO; (e) 10% Fe/SiO_2 from Gua + H_2 + CO_2. Dotted line represents Fe^{3+} species. See supplementary material for details on Mössbauer spectra fittings.

than 5% H_2O/50 mol% H_2) at 673 K on the pre-reduced catalyst. Under these conditions α-Fe is converted to Fe_3O_4 (see supplementary material). No conversion of guaiacol was detected on this oxidized catalyst. Benzene or toluene (the desired products) were never detected during all these experiments.

In order to clarify the role of each gas on the reaction, experiments were conducted on 10% Fe/silica catalyst with 50 mol% of H_2, 1% guaiacol, 5% of each (CH_4, H_2O, CO or CO_2) and rest Ar. Fig. 6 shows the conversion of guaiacol vs. time on stream for different gases composition. For guaiacol conversion under H_2 (50 mol%, rest Ar), 100% of guaiacol conversion is seen at the beginning of the run followed by a quick deactivation. As expected, the addition of CH_4 (Gua + H_2 + CH_4 in Figs. 6 and 7) leads to similar results. CH_4 has very few chemical effects on this reaction.

CO and H_2O slow down the reaction rate (Fig. 6) at the beginning of the run probably due to a fast deactivation of the catalyst by coking (from CO dismutation) and/or by sorption competitions on active sites. From 100 min time on stream, the conversion of guaiacol is similar with H_2 only or CO, H_2O or CH_4 (in H_2). In the case of Gua + H_2 + CO_2 we observed high initial conversion, comparable to Gua + H_2 experiment, but the deactivation of the catalyst is remarkably lower and the integral of converted guaiacol during 3 h increases. Guaiacol conversion is not stabilized after 3 h time-on-stream but is always higher than the ones of other experiments in Fig. 6.

Product yields (i.e. moles of *i* produced by mole of guaiacol converted) showed minor deviation upon time on stream (except for the high HDO conversion experiment, see Fig. 12). Fig. 7 shows the time-average yield of products from guaiacol conversion as a function of gas composition. TPO profiles of used catalysts are shown in Fig. 8. Table 4 displays the integral of CO_2 produced during TPO. In

Table 4
Results from integration of TPO curves for the conversion of CO and guaiacol under different gas mixtures, at 673 K, 1 atm, 80 mg 10% Fe/SiO_2.

Experiment	g C/100 g $_{\text{used catalyst}}$	C% yield mol C_{coke}/mol $C_{Gua\ converted}$
CO + H_2	23	–
Gua + H_2	10	5.7
Gua + H_2 + CH_4	11	7
Gua + H_2 + H_2O	4	4.5
Gua + H_2 + CO	19	21.7
Gua + H_2 + CO_2	13	5.8

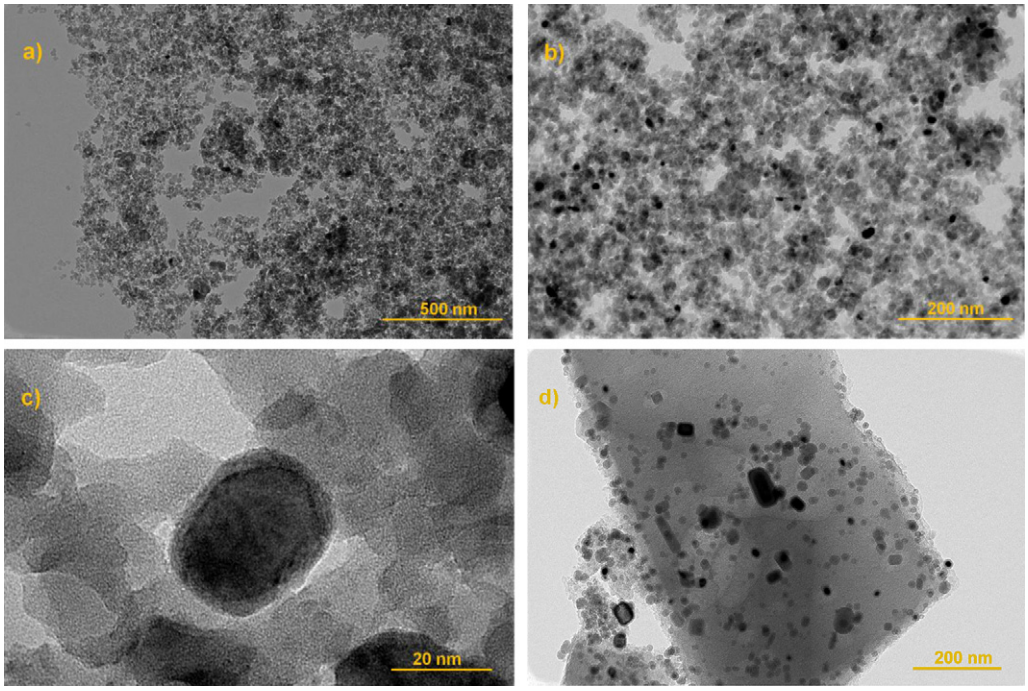

Fig. 3. TEM analysis of (a, b and c) 15% Fe/silica fresh passivated catalyst; (d) of 10% Fe/AC fresh passivated catalyst.

Fig. 7, coke and gases cannot be plotted in terms of yield (per converted guaiacol, Eq. (1)) because they can be produced from other species than guaiacol (CO, CO_2, etc.).

The presence of H_2O seems to reduce phenol conversion to benzene and toluene, and considerable amounts of catechol were produced (Fig. 7). Moreover, lack in products during Gua + H_2 + H_2O run (Fig. 7) should be attributed to non identified peaks on GC-FID, rather than gases and coke. Indeed, low carbon deposit was produced in the H_2O polluted experiment (Table 4). A GC–MS analysis of the solution recovered in the bubblers after the on-line sampling loop showed several aromatic compounds with two oxygen atoms like methyl di-hydroxy-benzene, methyl guaiacols and dimethoxy-benzene. The addition of other gases than H_2O leads to a lower effect in product selectivity (Fig. 7).

Two or three peaks (570–600 K, 630–670 K and 730–760 K) are evidenced on Fig. 8 (normalized TPO profiles) depending on gas composition. The low-temperature peak (570–600 K) seems to be related to guaiacol conversion because this peak is not seen with CO + H_2 mixture (without guaiacol) (Fig. 8). Gua + H_2

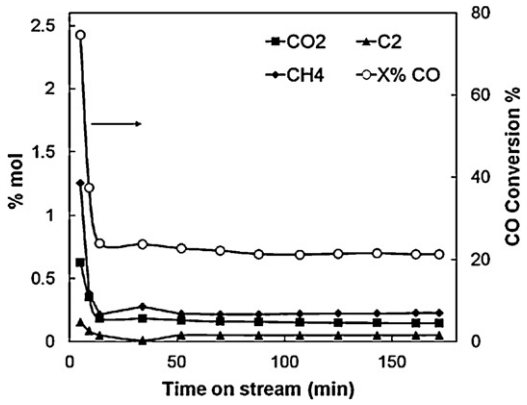

Fig. 5. Conversion and products of CO hydrogenation at 673 K, 1 atm, 5 mol% CO, 50% H_2, 80 mg of 10% Fe/SiO_2.

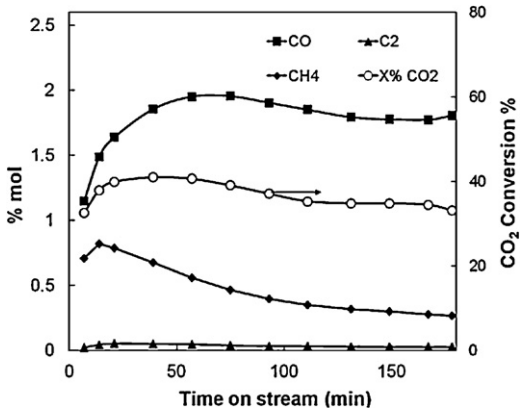

Fig. 4. Conversion and products of CO_2 hydrogenation at 673 K, 1 atm, 5 mol% CO_2, 50% H_2, 80 mg of 10% Fe/SiO_2.

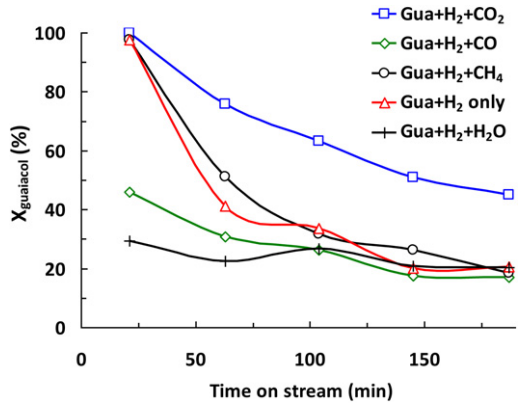

Fig. 6. Effect of gases on guaiacol conversion. (T = 673 K, P = 1 atm, 50 mol% H_2, 1% guaiacol, 5% extra gas (CH_4, H_2O, CO or CO_2) on 80 mg of 10% Fe/SiO_2.

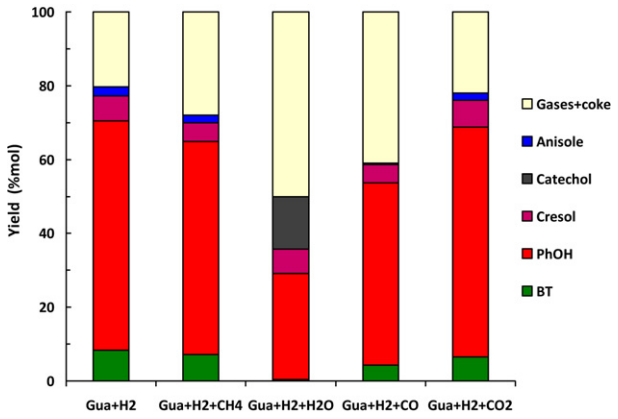

Fig. 7. Effect of gases on molar yield. (T = 673 K, P = 1 atm, 50 mol% H_2, 1% guaiacol, 5% extra gas (CH_4, H_2O, CO or CO_2) on 80 mg of 10% Fe/SiO_2. Gases and coke yield are calculated by difference.

showed similar profiles as Gua + H_2 + CH_4 and Gua + H_2 + CO_2 runs (Fig. 8) producing about the same C yield of coke (Table 4). With a Gua + H_2O + H_2 atmosphere, TPO profile displays mainly the low temperature and high temperature peaks. The CO_2 polluted experiment produced more coke than the reference run (Gua + H_2), but carbon yield is similar based on the mole of converted guaiacol. Indeed, integral conversion of guaiacol is higher with CO_2 + H_2 than with H_2 alone (Fig. 6). Gua + H_2 + CO experiment leads to a very big

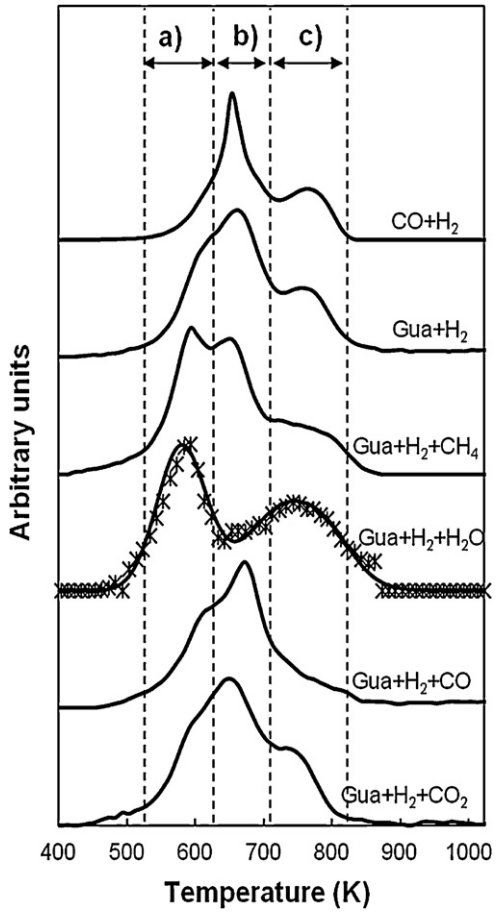

Fig. 8. TPO profiles of 10% Fe/SiO_2 catalyst used in guaiacol HDO (except for CO + H_2) after 3 h time on stream (1/WSHV = 0.6 g_{cat} h/g_{gua}, 50% H_2, 5% of H_2O, CO_2, CH_4 or CO). (a) Low temperature peak or shoulder; (b) middle temperature peak or shoulder; (c) high temperature peak or shoulder.

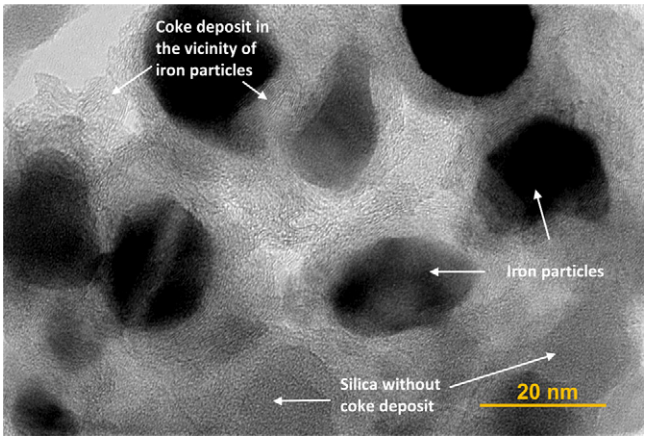

Fig. 9. TEM analysis of used catalyst (after guaiacol conversion with H_2 only). Carbon deposit (disordered carbon sheets) can be seen around iron particles on a silica colloidal matrix.

yield in carbon deposit (Table 4). If all the iron atoms are converted to carbide, carbon in carbide would be negligible compared with carbon deposit. The potential origins of the TPO peaks are examined in the discussion section.

TEM micrographs of Gua + H_2 + CO, Gua + H_2 + CO_2 and Gua + H_2 used catalysts showed carbon deposits (Fig. 9, Gua + H_2 only is shown). After observations of TEM micrographs, carbon deposit seems to be mainly formed in the vicinity of iron particles, and not on the whole silica surface. Such a deposit was not observed on Gua + H_2 + H_2O used catalyst. Average iron particle size remained stable after these runs.

In the absence of other gases than H_2, metallic iron (Fe) is the major phase (some oxidized speciation may be due to contact with air during storage) after guaiacol HDO [19]. XRD and Mössbauer spectroscopy were conducted to study the effect of gas composition on iron speciation (Fig. 2, Table 2 and see supplementary material). For the Gua + H_2 + CO used catalyst, iron was mainly converted into Hägg's carbide (χ-Fe_5C_2) and the Fe^{3+} species (Fig. 2d, Table 2). For the Gua + H_2 + CO_2 used catalyst, α-Fe remains the major species on molar basis (60%). χ-Fe_5C_2 and Fe^{3+} were also produced (Fig. 2e, Table 2). Fe^{3+} species were ascribed as small particles of Fe_3O_4 because typical Fe_3O_4 XRD signals are observed (see supplementary material).

After studying the individual effect of CO, CO_2, H_2O, CH_4 on guaiacol conversion under H_2 and spent catalysts composition (coke deposit and speciation of iron) for 10% Fe/SiO_2, the effect of all these gases as a whole mixture in the feeding stream on catalyst activity and composition has been studied. The effects of iron load and support have been also investigated with the complex gases mixture.

3.4. Effect of catalyst type (iron load and support) on guaiacol HDO in the presence of a model lignin pyrolysis gases

Nominal reactant mixture contained 50% H_2, 5% CO_2, 2% CO, 2% H_2O, 1% Guaiacol, and rest Argon and is referred as "Gua + H_2 + CO_2 + CO + H_2O". These proportions were chosen in order to mimic the real gas composition from lignin pyrolysis. In the study of the effect of individual gases, the same molar fraction (5 mol%) was used for each gas for a more rational comparison. This led of course to an overestimation of the effect of CO or H_2O when set at 2% in the gas mixture which mimics the real gas.

The four experiments with 3 different iron loads on silica (5, 10, 15 wt%) and 10% Fe over activated carbon (Figs. 10 and 11) were made with different mass of catalyst, but with the same iron surface (0.3 m^2 of iron) calculated from TEM images.

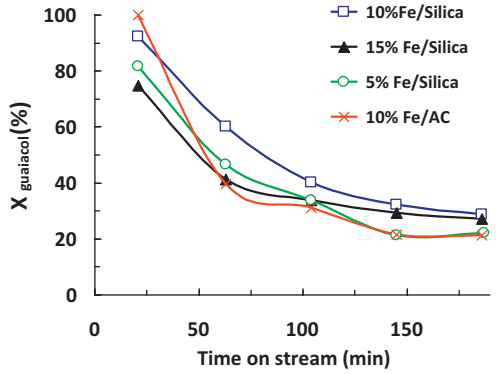

Fig. 10. Effect of support and iron load on guaiacol conversion. (T = 673 K, P = 1 atm, 50% H_2, 5% CO_2, 2% CO, 2% H_2O, 1% Guaiacol, rest Argon).

Fig. 10 shows the conversion of guaiacol on different catalysts. Only minor differences on guaiacol conversion as a function of time on stream can be seen for the 4 catalysts. Under the explored conditions, reactivity is roughly proportional to iron surface.

Product yields showed only minor deviation along the catalytic run. Fig. 11 displays the time-average yield of products for the 4 catalysts. The three silica-supported catalysts showed similar yields of aromatic hydrocarbons and phenols. However, carbon-supported catalyst produced almost no benzene and toluene and higher yield in catechol than silica-supported catalysts.

The TPO analysis of the 3 silica-supported used catalysts showed the same integral values of about 600 μmol_{Carbon} for the 3 runs.

3.5. High HDO conversion experiments

The conversion of guaiacol in the gas nominal mixture was studied on 1000 mg of 15% Fe/silica catalyst and 1200 mg of 10% Fe/AC. For both experiments guaiacol conversion was 100% all over time on stream. High mass of catalyst is needed to get a high selectivity in benzene (see [19] for more details about reaction pathways). The aim of these experiments is not to study the deactivation of catalyst based on guaiacol conversion but to investigate the evolution in benzene and phenol selectivity with time on stream. We previously justified the need of high guaiacol conversion to study benzene yield because one of the limiting step in the reaction pathways is phenol conversion [17].

Fig. 12 shows the products yield upon time on stream for the 15% Fe/silica catalyst. Initially, guaiacol is almost completely converted into Benzene and Toluene. Some important deactivation is

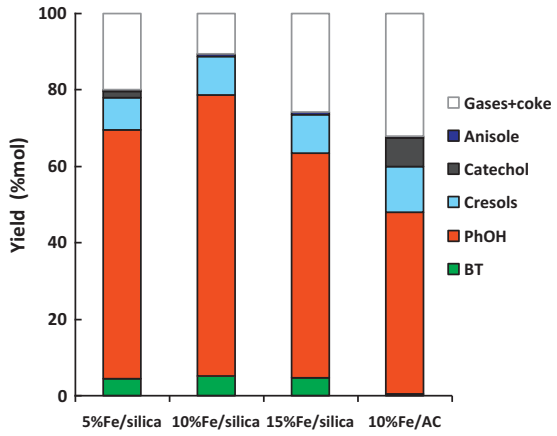

Fig. 11. Effect of support and iron load on yield. (T = 673 K, P = 1 atm, 50% H_2, 5% CO_2, 2% CO, 2% H_2O, 1% Guaiacol, rest Argon).

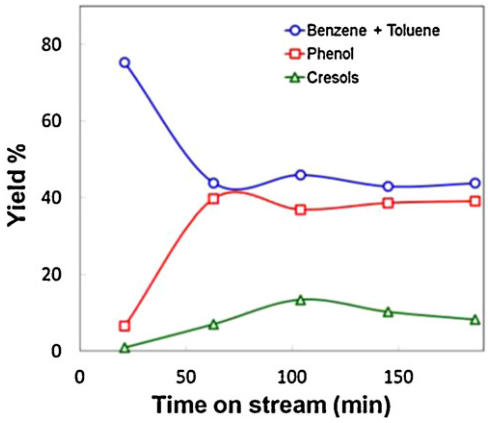

Fig. 12. Yield of products from guaiacol conversion on silica supported iron catalyst (1000 mg, 7.5 g_{cat} h/g_{gua} 15% Fe/SiO_2, T = 673 K, P = 1 atm, 50% H_2, 5% CO_2, 2% CO, 2% H_2O, 1% Guaiacol, rest Argon).

observed on the first hour of the run, and then conversion and selectivity are stable during 2 h. This result shows that Fe/silica catalyst is active and selective for guaiacol HDO in the gas phase even in presence of H_2, CO, CO_2 and H_2O. The next step of our work will be to test this catalyst on a real lignin pyrolysis gas.

XRD and Mössbauer analyses of this catalyst (Table 2, Fig. 2c) showed the coexistence of χ-Fe_5C_2, α-Fe, and Fe^{3+} species identified as small Fe_3O_4 particles on XRD. The major phase remains α-Fe on a molar basis (48%). 40% of the Mössbauer spectrum area remains unexplained. More fundamental research is needed to clarify the oxidation state of iron species in this system. However, we may think that it probably corresponds to different "magnetites" with various grain sizes (see supplementary material).

Fig. 13 shows the product from guaiacol HDO on 10% Fe/AC catalyst as a function of time on stream. Guaiacol is hydrodeoxygenated partially to phenol and cresol, but the following reactions from phenol and cresols to benzene and toluene did not happen. The selectivity in phenol and cresols even increases during the first hour and is then well stable.

4. Discussion

4.1. Iron species

The XRD and Mössbauer analyses show that iron may exist in reduced (metallic, carbidic) or oxidized state (Fe_2O_3, Fe_3O_4) as a

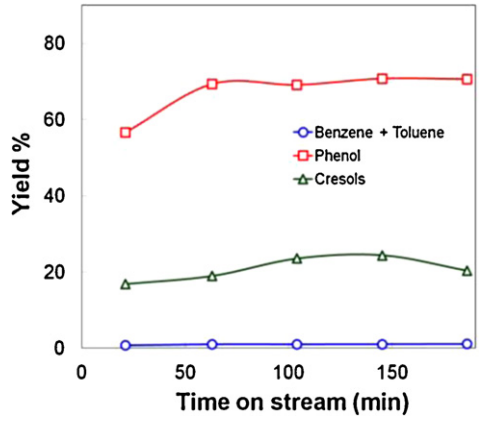

Fig. 13. Yield of products from guaiacol conversion on carbon supported iron catalyst (1200 mg, 9 g_{cat} h/g_{gua} 10% Fe/AC, T = 673 K, P = 1 atm, 50% H_2, 5% CO_2, 2% CO, 2% H_2O, 1% Guaiacol, rest Argon).

function of gases composition. The iron carbide is formed due to interaction with carbonaceous surface species. Presence of iron oxides is attributed, not only to passivation and exposure to air during storage, but also to deactivation of metallic iron throughout oxidation processes by phenols, water, carbon oxides. Therefore, catalyst deactivation is believed to be due to both iron oxidation and carbon deposit. The amorphous carbon phase (Fig. 9) could also be produced by iron carbide oxidation during passivation or storage [29]. Nevertheless, only a minor part of carbon deposit would be under the form of carbide even if iron is entirely carburized (from molar calculation). The faster deactivation with CO and H_2O (Fig. 6) could be due to carburization (high amount of χ-Fe_5C_2 analyzed in Table 2) and oxidation respectively. Nevertheless, the catalyst is still active after 3 h time on stream even with CO or H_2O.

If the gas composition favours the formation of Fe_3O_4 instead of Fe, the activity disappears (tested with H_2/H_2O mixture). It seems thus more probable that a reduced iron is needed to be active.

The presence of α-Fe after 3 h (Table 2) leads to a higher conversion of guaiacol with CO_2 experiment (Fig. 6). Consequently, α-Fe would be a more active iron species than χ-Fe_5C_2. Iron carbide could be an active phase as generally mentioned for Fisher-Tropsch synthesis [29]. Furthermore, Mössbauer spectroscopy only gives the bulk composition of iron species and not the composition of surface-iron. Iron particles could be in the form of grains with layers of different speciations, H and C species could diffuse through these layers. It is also possible that a metallic core can remain even when the surface is totally oxidized or carburized. Residual α-Fe or other speciations could also be present but not detected by Mössbauer (if inferior to about 5 wt%). This could be the case for the experiment Gua + H_2 + CO (Figs. 6 and 7) where Fe^{3+} and χ-Fe_5C_2 were detected but not α-Fe.

4.2. Reaction mechanisms

In our previous study with Fe/SiO_2 [19] we proposed a bifunctional catalysis for the gas phase HDO of guaiacol in the presence of H_2. It would also hold for 15% Fe/AC examined in the present study. Reduced iron phases would be the active phase, the main role of which being to activate H_2. The support offers the acid actives sites on which the guaiacol molecule adsorbs and then reacts with H-spiltover species coming from dihydrogen dissociated on the reduced iron sites. The C_{arom}—O linkage (present in guaiacol, phenol, catechol, etc.) could be activated via adsorption on silanols as proposed by Popov et al. [30] or via the acidic functionalities of activated carbon [26]. This means that the overall reaction rate is controlled by both the stability of the chemisorbed oxygenate species and the rate of the C_{arom}—O bond breaking [32]. The bifunctional mechanism was used in literature to explain HDO of guaiacol and other phenolic compounds [5,17,32–34]. Laurent and Delmon demonstrated the high importance of the interactions between metals and support [33].

Fe/SiO_2-catalysed HDO of guaiacol (that is a set of complex reactions) mainly occurs through the hydrogenolysis of the $C_{aromatic}$—O bonds in hydroxyl or methoxyl groups [19]. Many other reactions may happen (transalkylation, ring hydrogenation, dehydration, dehydrogenation, etc.). Bui et al. proposed a general reaction network, but they found that using $CoMoS/ZrO_2$ catalyst (40 atm, 573 K), observed products lead to a network as simple as guaiacol to phenol to benzene [18]. An interesting and complete reaction network was developed and fitted for gas-phase guaiacol HDO on Pt/Al_2O_3 (1 atm, 573 K) by Nimmanwudipong et al. [35].

Transalkylation occurs in our experiments. Cresols and/or toluene were produced in every runs (always less than phenol or benzene).

Phenol is the main intermediate product in our case and is easily formed from guaiacol demethoxylation (hydrogenolysis of $C_{aromatic}$—methoxy bond). The potential competitive route for guaiacol conversion to phenol through hydrogenation of aromatic ring/demethoxylation/dehydrogenation is less likely to happen on an iron based catalyst. Similarly, phenol conversion to benzene through the same processes (through hydrogenation of the aromatic ring) is not likely to occur. Indeed, Emmett and Skau [36] detected no activity for benzene hydrogenation at 673 K working with Fe. Lately, Yoon and Vannice [37] measured a relatively low activity of Fe for benzene hydrogenation compared to other transition or precious metals (Ni, Co). Competitive hydrogenation of the aromatic ring of phenol was reported for Ni/SiO_2 catalysts [11,38]. To our best knowledge, it has not been reported for iron based catalysts. Iron is a trade-off between activity and selectivity. This is the reason why we chose iron as the active phase in the guaiacol HDO, expecting minimum aromatic ring hydrogenation. Ring hydrogenated products (cyclohexane, cyclohexenes, cyclohexanols) were not detected in our experiments. There could be also a competition between HDO of phenol to form benzene and H_2O (through hydrogenolysis of $C_{aromatic}$—OH) and phenol conversion to C_5 species (and CO) that could be coke precursors [39].

4.3. Coke deposits

Relation exists between support acidity and cracking and coking [40,41]. Centeno et al. [42] showed that, during HDO of guaiacol much less coke is deposited on silica supported and unsupported CoMo catalysts as compared to alumina supported catalysts. Moreover, coke deposit mainly occurs on alumina for CoMo-alumina catalysts and support acidity plays an important role in its formation. Guaiacol conversion is highly inhibited by ammonia and catalytic activity decreases for potassium-modified catalysts [33,42]. Cracking and coking also occur on acidic zeolites in the absence of a metal promoter [43].

Observations of TEM images in this study showed that carbon deposits are formed mainly in the vicinity of iron particles (Fig. 9). It was never observed on silica colloids without iron. Absence of coking on bare silica is related to its low acidity. Guaiacol molecule may also adsorb and react with iron species, producing coke without the help of the support.

4.4. Effect of support

Under our nominal conditions (50% H_2, 5% CO_2, 2% CO, 2% H_2O, 1% Guaiacol, rest Argon), 10% Fe/AC catalyst also showed a very low yield of benzene and toluene compared to silica-supported catalyst, and consequently high yield of phenol (Figs. 12 and 13). Phenols would be not enough stably adsorbed on the carbon support for further HDO to aromatic hydrocarbons. They are desorbed much more rapidly than on the silica support. Activated carbon is a complex support. Both acid and basic functionalities of different chemistry could be initially present, or generated at 673 K on activated carbon surface in the presence of H_2O and CO_2 [26,31]. More fundamental research is needed to explain this selectivity as compared to that of silica. Influence of support nature on selectivity was also observed by Bui et al. [17]. They obtained a good selectivity to benzene instead of ring hydrogenation products using ZrO_2 as support for CoMoS instead of TiO_2 or Al_2O_3.

4.5. Individual effect of gases

It should be first noticed that CO and H_2O (both in H_2) have mainly an effect on the initial conversion of guaiacol compared with H_2 only (Fig. 6) showing an effect on the deactivation rate rather than on long term activity. After 100 min time on stream, the conversion of guaiacol is similar for all gases except for CO_2. With CO_2 (in H_2) the conversion is higher but not yet completely stable after

3 h time on stream. Longer time on stream experiments are needed to investigate stable conversion with CO_2.

Water has a negative effect on HDO initial activity and on the selectivity of the catalyst (Figs. 6 and 7). Decreased initial activity could be due to some oxidation of iron active site. It can also be explained through silanols activation. H_2O molecules may compete for silanols adsorption sites and, in the mean time, make the desorption of phenolic molecules faster than HDO of C_{arom}—O linkage. This explains the low conversion and the high yields to catechol and other highly-oxygenated molecules by hydrolysis. Zhu et al. [13,15] found similar results concerning selectivity change to hydrolysis products working on anisole catalytic reactions over zeolites (and Pt/HBeta catalyst). Shin and Keane [11] studied the hydrogenation of phenol on Ni/SiO_2 at 573 K. In the presence of H_2 and CH_3OH, phenol is converted to benzene; but in the presence of H_2 and H_2O, cyclohexanone was also produced and benzene yield decreased. Those results are consistent with our finding.

CO_2 has a very positive effect to reduce deactivation. Coke deposit yield based on converted guaiacol (Table 4) was almost not changed (compared with Gua + H_2 without CO_2). A possible explanation is that CO_2 impedes the formation of coke especially in the vicinity of the reactive sites, probably by H_2O molecules produced by the reverse water–gas shift reaction (WGSR) [28]. Indeed, water addition was shown to impede coke formation (Fig. 8). Moreover, the amount of water produced by the reverse WGSR (around 0.5%) could be too low to slowdown the HDO reaction rate. In other words, in the presence of CO_2, there are enough H_2O molecules formed to reduce coke from useful active sites but not enough to affect phenolic molecules sorption. If this explanation is true, there should exist an optimum concentration of water on the gas phase that reduces coking without decreasing catalyst activity and selectivity.

The formation of carbide represents a negligible amount of carbon deposit on the Gua + H_2 + CO spent catalyst. Consequently, the TPO pattern for guaiacol conversion with CO (and H_2) could be mainly attributed to coke formation from heavy hydrocarbons from CO hydrogenation. Galuszka et al. [23] showed by infrared analysis coupled to TPO and Mössbauer analysis that the carbonaceous deposit on Fe/SiO_2 (after Fisher-Tropsch synthesis) is likely composed of aliphatic, carbidic and amorphous forms of deposit. The two types of carbonaceous deposit analyzed in our case (for CO + H_2 conversion without guaiacol, Fig. 8) may come from aliphatic and amorphous species since the carbide contribution to carbon deposit is negligible. When guaiacol is added to H_2 + CO, a third peak on the TPO curve appears at low temperatures probably from an oxygenated form of the carbonaceous deposit [23], formed from phenolic species conversion.

From Mössbauer spectroscopy (Fig. 2c, Table 2), it is shown that, with the nominal gases composition (Gua + H_2 + CO + CO_2 + H_2O), metallic iron is still the major iron species (on a molar basis). These gases composition and experimental conditions are sufficiently reducing to maintain a suitable fraction of reduced–active iron and especially of metallic iron.

4.6. High HDO conversion reactions

Fig. 12 shows that Fe/SiO_2 catalyst can be used for the HDO of model lignin pyrolysis vapours into BTX, even in the presence of CO, CO_2 and H_2O (66% of BT Carbon yield).

It is very difficult to compare our result with literature because conditions and/or goals were not always the same. Table 1 is far from being exhaustive. The result from Gonzalez-Borja and Resasco [14] on bimetallic Pt-Sn/Carbon Nanofiber/Inconel monolith was selected because their conditions were similar to ours. They found similar selectivity and higher activity with the drawback of using Pt. Shin and Keane obtained 99% of benzene from phenol on 20% Ni/SiO_2 at lower temperature (573 K). We did not tested nickel because it could convert guaiacol to methane at 673 K [37]. High-pressure liquid phase data is less comparable. Good yield in aromatic hydrocarbons from depolymerised lignin (base-catalysed) have been obtained with sulphided Mo catalysts promoted by Fe or other metals [44].

Fig. 13 shows the phenol and cresol yield for Fe/AC catalyst in a very high HDO conversion experiment. Guaiacol is fully converted to mono-oxygenated aromatic molecules (phenol), but those valuable molecules are not further hydrogenated. This is a very important result for researchers looking to produce phenols from lignin pyrolysis vapours. Very oxygenated aromatic molecules could be converted to less oxygenated, more stable and value-added phenols directly from lignin vapours catalytic treatment. Activated carbon was also chosen based on its potential benefit for support and iron regeneration and recovery (by coke and support oxidation). Activated carbon or char can be produced from the pyrolysis process. The support catalyst could be thus produced and regenerated in the process itself [45–47]. Regeneration of iron/AC and recovery strategies of iron are still needed to be looked for.

5. Conclusions

For a better understanding of the guaiacol HDO on iron supported catalysts, the individual behaviour of gases (CO, CO_2, CH_4, and H_2O) was investigated. XRD and Mössbauer analyses are both needed to investigate iron speciations.

Methane has few effects on guaiacol HDO contrary to the other gases. Water strongly inhibits the overall activity but increases production of phenols instead of benzene through the hydrolysis of the adsorbed precursors. Carbon monoxide has a strong negative effect on initial reaction rate due to carburization of iron and formation of an important yield of coke. Carbon dioxide has a very positive effect on guaiacol HDO reaction reducing deactivation.

Under the lignin pyrolysis model mixture (Gua + H_2 + CO + CO_2 + H_2O), 15% Fe/SiO_2 was active and selective for the production of benzene and toluene with no ring hydrogenation (66% of carbon yield of BT, 1/WHSV = 7.5 h). α-Fe remains in the catalyst with this gas mixture. Fe^{3+}, Fe_3O_4 and Fe_5C_2 were also observed. 10% Fe/AC was active and selective for phenol and cresols production from guaiacol.

Coke was shown to deposit in the vicinity of iron particles. This finding suggests that the HDO occurred at the metal–support interface.

The above conclusions prompt us to undertake in the next future the investigation of these catalysts on real pyrolysis gases.

Appendix A. Supplementary data

Supplementary data associated with this article can be found, in the online version, at http://dx.doi.org/10.1016/j.apcatb.2012.09.043.

References

[1] J. Holladay, J. Bozell, J. White, D. Johnson, Top Value-Added Chemicals from Biomass Volume II—Results of Screening for Potential Candidates from Biorefinery Lignin. Report of the PNNL, U.S. Department of Energy, 2007.
[2] P. de Wild, R. Van der Laan, A. Kloekhorst, E. Heeres, Environmental Progress and Sustainable Energy 28 (2009) 461.
[3] B. Scholze, C. Hanser, D. Meier, Journal of Analytical and Applied Pyrolysis 58–59 (2001) 387.
[4] B. Scholze, D. Meier, Journal of Analytical and Applied Pyrolysis 60 (2001) 41.
[5] E. Furimsky, Applied Catalysis A 199 (2000) 147.
[6] D.C. Elliott, Energy and Fuels 21 (2007) 1792.
[7] R.N. Olcese, M. Bettahar, D. Petitjean, J.-C. Moise, A. Dufour, First International Congress on Catalysis for Biorefineries (CatBior), Torremolinos-Malaga, Spain, 2011, pp. 288–293.

[8] L. Abdelouahed, O. Authier, G. Mauviel, J.P. Corriou, G. Verdier, A. Dufour, Energy and Fuels 26 (6) (2012) 3840.
[9] C. Pirez, M. Capron, H. Jobic, F. Dumeignil, L. Jalowiecki, A. Duhamel, Angewandte Chemie International Edition 50 (2011) 10193.
[10] R.D. Cortright, J.A. Dumesic, Low-temperature hydrogen production from oxygenated hydrocarbons, U.S. Patent 6699457 (2004).
[11] E.-J. Shin, M.A. Keane, Industrial and Engineering Chemistry Research 39 (2000) 883.
[12] N. Mahata, K.V. Raghavan, V. Vishwanathan, M.A. Keane, Reaction Kinetics and Catalysis Letters 72 (2001) 297.
[13] X. Zhu, R.G. Mallinson, D.E. Resasco, Applied Catalysis A 379 (2010) 172.
[14] M.A. Gonzalez-Borja, D.E. Resasco, Energy and Fuels 25 (2011) 4155.
[15] X. Zhu, L.L. Lobban, R.G. Mallinson, D.E. Resasco, Journal of Catalysis 281 (2011) 21–29.
[16] Y. Zhao, L. Deng, B. Liao, Y. Fu, Q.-X. Guo, Energy and Fuels 24 (2010) 5735.
[17] V.N. Bui, D. Laurenti, P. Delichere, C. Geantet, Applied Catalysis B 101 (2010) 246.
[18] V.N. Bui, D. Laurenti, P. Afanasiev, C. Geantet, Applied Catalysis B 101 (2011) 239.
[19] R.N. Olcese, M. Bettahar, D. Petitjean, B. Malaman, F. Giovanella, A. Dufour, Applied Catalysis B 115–116 (2012) 63.
[20] B. Valle, A.G. Gayubo, A.T. Aguayo, M. Olazar, J. Bilbao, Energy and Fuels 24 (2010) 2060.
[21] J. Carignan, P. Hild, G. Mevelle, J. Morel, D. Yeghicheyan, Geostandards Newsletter 25 (2007) 187.
[22] J. Rodríguez-Carvajal, Physica B: Condensed Matter 192 (1993) 55.
[23] J. Galuszka, T. Sang, J.A. Sawicki, Journal of Catalysis 136 (1992) 96.
[24] B. Kalska-Szostko, M. Zubowska, D. Satula, Proceedings of the XL Zakopane School of Physics, Poland, 2006, pp. 365–369.
[25] R.E. Vandenberghe, I. Nedkov, T. Merodiiska, L. Slavov, Hyperfine Interactions 165 (2006) 267.
[26] C. Sepúlveda, K. Leiva, R. García, L.R. Radovic, I.T. Ghampson, W.J. DeSisto, J.L.G. Fierro, N. Escalona, Catalysis Today 172 (2011) 232.
[27] A.A. Chen, M.A. Vannice, J. Phillips, Journal of Physical Chemistry 91 (1987) 6257.
[28] G.D. Weatherbee, C.H. Bartholomew, Journal of Catalysis 87 (1984) 352.
[29] S. Janbroers, J.N. Louwen, H.W. Zandbergen, P.J. Kooyman, Journal of Catalysis 268 (2009) 235.
[30] A. Popov, E. Kondratieva, J.M. Goupil, L. Mariey, P. Bazin, J.-P. Gilson, A. Travert, F. Mauge, Journal of Physical Chemistry C 114 (2010) 15661.
[31] F. Rodríguez-reinoso, Carbon 36 (1998) 159.
[32] G. Neri, A.M. Visco, A. Donato, C. Milone, M. Malentacchi, G. Gubitosa, Applied Catalysis A 110 (1994) 49.
[33] E. Laurent, B. Delmon, Industrial and Engineering Chemistry Research 32 (1993) 2516–2524.
[34] M.A. Keane, R. Larsson, Catalysis Letters 129 (2009) 93.
[35] T. Nimmanwudipong, R. Runnebaum, D. Block, B. Gates, Catalysis Letters 141 (2011) 779.
[36] P. Emmett, N. Skau, Journal of the American Chemical Society 65 (1943) 1029–1035.
[37] K.J. Yoon, M.A. Vannice, Journal of Catalysis 82 (1983) 457.
[38] S.G. Shore, E. Ding, C. Park, M.A. Keane, Catalysis Communications 3 (2002) 77–84.
[39] R. Cypres, Fuel Processing Technology 15 (1987) 1.
[40] J.F.L. Page, Catalyse de Contact: Conception, Préparation et Mise en oeuvre des Catalyseurs Industriels, Editions TECHNIP, France, 1978.
[41] P. Marecot, H. Martinez, J. Barbier, Journal of Catalysis 138 (1992) 474.
[42] A. Centeno, E. Laurent, B. Delmon, Journal of Catalysis 154 (1995) 288.
[43] A.G. Gayubo, A.T. Aguayo, A. Atutxa, R. Prieto, J. Bilbao, Energy and Fuels 18 (2004) 1640.
[44] J.S. Shabtai, W.W. Zmierczak, E. Chornet, D. Johnson, Process for converting lignins into a high octane blending component, Patent US20030115792 (2003).
[45] A. Dufour, A. Celzard, V. Fierro, E. Martin, F. Broust, A. Zoulalian, Applied Catalysis A 346 (2008) 164.
[46] Z. Min, P. Yimsiri, M. Asadullah, S. Zhang, C.-Z. Li, Fuel 90 (2011) 2545.
[47] J. Rodriguez-Mirasol, T. Cordero, J.J. Rodriguez, Energy and Fuels 7 (1993) 133.